Ab initio investigation of magnetic ordering in the double perovskite Sr_2NiWO_6

Nafise Rezaei,[1,*,†] Tayebehsadat Hashemifar,[1,2,†] Mojtaba Alaei,[1] Farhad Shahbazi,[1] S. Javad Hashemifar,[1] and Hadi Akbarzadeh[1]

[1]*Department of Physics, Isfahan University of Technology, Isfahan 84156-83111, Iran*

[2]*Department of Physics, Faculty of Science, Shahrekord University, Shahrekord 88186-34141, Iran*

(Received 25 June 2018; revised manuscript received 12 January 2019; published 8 March 2019)

Ab initio calculations, the generalized gradient approximations (GGA/GGA+U), are used to propose a spin Hamiltonian for the B-site ordered double perovskite Sr_2NiWO_6. Our results show that the exchange interaction constants between the next-nearest neighbors in both intra- and inter-ab planes (J_2 and J_{2c}) are an order of magnitude larger than the ones between the nearest neighbors (J_1 and J_{1c}). Employing the Monte Carlo simulation, we show that the obtained Hamiltonian properly describes the finite-temperature properties of Sr_2NiWO_6. Our *ab initio* calculations also reveal a small magnetic anisotropy and nontrivial biquadratic interaction between the nearest inter-ab plane neighbors, which play essential roles in stabilizing the type-II antiferromagnetic ground state of Sr_2NiWO_6.

DOI: 10.1103/PhysRevB.99.104411

I. INTRODUCTION

Ordered double perovskites with a general chemical formula $A_2BB'O_6$ have received great attention owing to the magnetic interactions tunable by substitutions on B and B' ions [1–3]. For instance, the substitution of Mo by W in Sr_2CuMoO_6 tends to decrease the Curie-Weiss temperature from -116 to -300 K [4]. The wide variety of $A_2BB'O_6$ compounds with different A, B, and B' ions represents various novel properties such as colossal magnetoresistance in Sr_2FeMoO_6 [5], half-metallicity in Sr_2CrWO_6 [6], multiferroics in Sr_2NiMoO_6 [7–9] and Pb_2FeMeO_6 (Me = Nb, Ta, Sb) ceramics [10,11], photovoltaics in Bi_2FeCrO_6 [12] and Sc_2FeCrO_6 [13], and low-dimensional antiferromagnetic (AFM) behavior in $Ba_2CuB'O_6$ and $Sr_2CuB'O_6$ (B' = W, Te) compounds [14].

In the majority of magnetic ordered double perovskites $A_2BB'O_6$, the B site, B' site, or both could be occupied by transition-metal magnetic ions. For the cases where B is magnetic and B' is a diamagnetic ion, the magnetic ions interact with each other through B-O-B'-O-B bonds (Fig. 1). The magnetic B ions can interact with each other through direct and superexchange interactions. Due to the large distance between the B ions the direct exchange interaction is negligible, hence the dominant magnetic interaction would be the superexchange interaction mediated by the B' and O ions. The B-B'-B angle is 90° for the nearest and 180° for the next-nearest neighbors (Fig. 1), which could make the nearest-neighbor (NN) superexchange interaction much smaller than the next-nearest-neighbor (NNN) interaction. The dependence of the superexchange interaction on the bond angle is given by the Goodenough-Kanamori-Anderson rules [15,16], according to which the superexchange is AFM and its strength is maximum for a 180° bond angle.

Typically, ordered double perovskites show low-temperature AFM ordering, except for some compounds including the La_2BMnO_6 (B = Mg,Co,Ni,Cu) group which represent ferromagnetic (FM) ordering [17].

Sr_2NiWO_6 is a B-site ordered double perovskite in which the magnetic Ni^{+2} ion resides on the B site and the hexavalent diamagnetic W^{+6} ion occupies the B' locations. Its crystalline structure at room temperature is tetragonal and transforms to the cubic symmetry above 520 K. The lattice distortion tilts the Ni-O-W angle from 180° to 165° in the ab plane [18]. Sr_2NiWO_6 exhibits a sharp transition to a type-II AFM (AFM-II) spin ordering below the Néel temperature 54 K [18,19]. Analysis of the spin-wave excitation spectrum indicates that the 90°superexchange interaction in Sr_2NiWO_6 is much smaller than the 180° one [20,21]. On the contrary, Iwanaga *et al.* argued that these magnetic interactions in Sr_2NiWO_6 are comparable [18]. Hence, the relative strength of these superexchange interactions in Sr_2NiWO_6 is a matter of dispute. Furthermore, the existence of a sharp peak in the magnetic susceptibility of Sr_2NiWO_6, unlike Sr_2CuWO_6, is an indication of a three-dimensional ordering in this compound.

The frustration of the exchange interactions between the spins could lead to magnetic degeneracy in antiferromagnetic materials. The fcc magnetic lattice with antiferromagnetic NN and NNN interactions is an example of frustrated magnets. This lattice is composed of four Heisenberg antiferromagnetic cubic sublattices, in such a way that the sum of the first neighboring ion magnetic fields at a given site vanishes. This results in four independent magnetic sublattices with AFM ordering. The magnetic moment directions of the sublattices are not constrained on each other. Such a freedom to select the relative magnetic moment direction can be lifted by including some higher-order exchange interactions such as biquadratic interactions or single-ion interactions generated by the spin-orbit effect. Neglecting the small tetragonal distortion in ordered double perovskites such as Sr_2NiWO_6, the

*n-rezaee@ph.iut.ac.ir

†These authors contributed equally to this work.

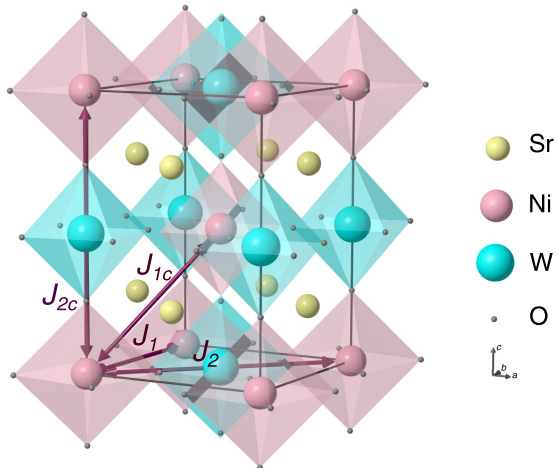

FIG. 1. Crystal structure of Sr_2NiWO_6. The thick violet arrows show the nearest and next-nearest neighbors at the intra-*ab* plane (J_1 and J_2) and inter-*ab* plane (J_{1c} and J_{2c}), respectively [22].

magnetic lattice turns out to be fcc, hence one expects the emergence of frustration in these compounds. In this paper, we study Sr_2NiWO_6 as a prototype of a (rocksalt) ordered double perovskite to shed light on the magnetic features of these compounds. Moreover, the experimental spin-wave excitation spectrum obtained for Sr_2NiWO_6 [20,21] will help us to compare the parameters of our spin Hamiltonian with those extracted by fitting the spin-wave spectrum using linear spin-wave theory.

In this study, we employ density functional calculations including the Hubbard correction to build a spin model Hamiltonian for Sr_2NiWO_6. We show that the NNN exchange couplings between the intra- and inter-*ab* plane Ni ions are in the same order, which guarantees the three-dimensional magnetic ordering in Sr_2NiWO_6. We also discuss the thermodynamic properties of the obtained model Hamiltonian using the classical Monte Carlo (MC) simulation. In addition to the Heisenberg exchange couplings, we consider the biquadratic magnetic interaction and magnetic anisotropy interaction in the spin Hamiltonian and argue the key role of these interactions in finding the correct magnetic ground state of Sr_2NiWO_6.

The paper is organized as follows. Section II discusses the *ab initio* methods to construct the spin Hamiltonian and also the details of the MC simulation. The results and discussions are given in Sec. III, and Sec. IV is devoted to the conclusions.

II. METHOD

The major parts of the *ab initio* calculations were done by the QUANTUM ESPRESSO (QE) package [23], which is based on density functional theory (DFT). To treat the electron-nucleus interaction, the projector augmented-wave (PAW) pseudopotentials were employed. The exchange-correlation potential was approximated by the Perdew-Burke-Ernzerhof (PBE) functional within the generalized gradient approximation (GGA) [24]. To improve the on-site Coulomb repulsion of the localized d electrons, we have applied the GGA+U method in a simplified approach by Dudarev [25], which only needs an effective Hubbard parameter (U_{eff}). We used $8 \times 8 \times 6$ k-point meshes for Brillouin zone sampling of the primitive unit cell (which contains two formula units). The experimental crystal structure was taken from Ref. [18]. An energy cutoff of 40 Ry (440 Ry) was chosen for the wave-function (electron density) expansion in the plane-wave basis set. Higher-energy cutoffs were chosen for the lattice and site geometry optimizations (50 and 550 Ry for the wave-function and density expansions, respectively). We have estimated the U_{eff} parameter by using the linear response (LR) method [26]. For these calculations, a $2 \times 2 \times 2$ supercell, containing 16 Ni atoms, was used. We employed the full-potential linearized augmented plane-wave (LAPW) method, using the FLEUR code [27], to verify the PAW pseudopotentials. For the LAPW calculation, we set $k_{\max} = 4.5$ a.u.$^{-1}$, and we chose 2.0, 2.0, 2.2, and 1.4 a.u. for the muffin-tin radii of Sr, Ni, W and O, respectively.

To find an effective spin Hamiltonian, the collinear spin-polarized DFT results were mapped to the Heisenberg Hamiltonian given by

$$H = -\frac{1}{2}\sum_{i,j} J_{ij}\hat{\mathbf{n}}_i \cdot \hat{\mathbf{n}}_j, \tag{1}$$

where $\hat{\mathbf{n}}_i$ denotes a unit vector in the direction of the magnetic moment at the ith lattice site, and J_{ij}'s are Heisenberg exchange constants describing the strength of the magnetic coupling between the magnetic ions residing on the ith and jth sites. To derive the exchange constants, the DFT total energies of various magnetic configurations were calculated. Then, by employing the least-squares method, the NN and NNN exchange couplings at the intra-*ab* plane (J_1 and J_2) and inter-*ab* plane (J_{1c} and J_{2c}) were computed (Fig. 1).

For the Ni ion with $S = 1$, a biquadratic interaction $\sum_{i>j} B_{ij}(\hat{\mathbf{n}}_i \cdot \hat{\mathbf{n}}_j)^2$ is also expected [28]. To estimate the biquadratic couplings B_{ij}, we used the LAPW FLEUR code [27] which is more specialized for noncollinear spin-polarized DFT. Because of the existence of the heavy element W in Sr_2NiWO_6, we investigated the effect of the magnetic anisotropy, $\Delta\sum_i(\hat{\mathbf{n}}_i \cdot \hat{\mathbf{z}})^2$, where Δ denotes the strength of the anisotropy. These calculations also were done within the LAPW method by including the spin-orbit coupling (SOC) and Hubbard correction (GGA+U+SOC).

In the end, we have used classical MC simulations to investigate the finite-temperature properties of the obtained spin Hamiltonian. The parallel tempering MC method was carried on a lattice size $N = 2 \times 12^3$, and a uniform temperature range including 64 temperatures was selected. We used 1×10^6 MC steps per spin for equilibration and 1×10^6 MC steps for sampling. To reduce the correlation between the data, we skipped ten MC steps between the data collections. In a parallel tempering algorithm, we allowed the spin configurations at the different temperatures to swap with each other after ten MC steps.

III. RESULTS AND DISCUSSION

A. Spin Hamiltonian

Sr_2NiWO_6 crystallizes in the tetragonal space group $I4/m$ with cell parameters ($a = 5.5571$, $c = 7.9133$ Å) [18]. As

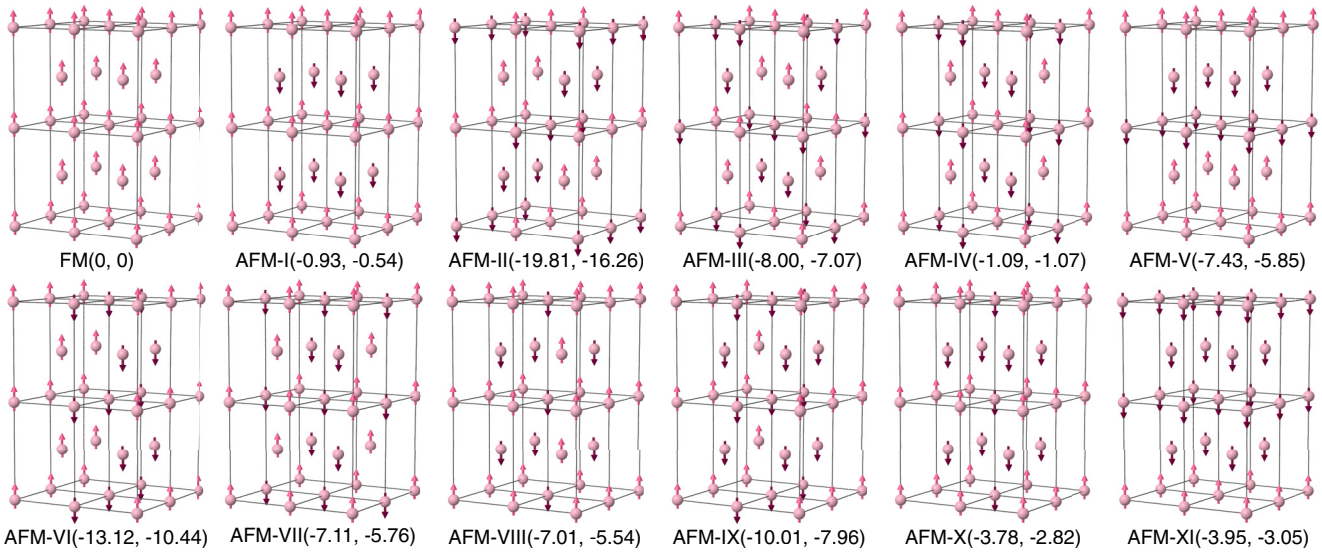

FIG. 2. Schematic representation of the Ni spin moments in the various magnetic configurations used for calculating the exchange constants. The numbers in parentheses are the total energy difference of each magnetic configuration (meV/f.u.) with respect to the ferromagnetic (FM) configuration for $U_{\text{eff}} = 5$ and 4.72 eV, respectively.

shown in Fig. 1, the transition-metal ions including the magnetic Ni^{+2} ions and nonmagnetic W^{+6} ions are located at the center of the oxygen octahedra. In order to have insight into the DFT magnetic ground state, different magnetic configurations are considered, as presented in Fig. 2. The calculations are performed within GGA, and GGA+U approximations for the experimentally identified as well as *ab initio* optimized crystal structures. For any on-site Hubbard parameter U_{eff} varying from 0 to 7 eV, the magnetic ground state of Sr_2NiWO_6 is the AFM-II ordering (Fig. 2), consistent with the experimental observation [20,21]. In AFM-II, each Ni ion aligns its moment parallel to half and antiparallel to the other half of its nearest neighbors, whose number is 4 in the *ab* plane and 8 out of plane. However, for both the intra- and inter-*ab* plane NNNs, the directions of the magnetic moments are antiparallel (Fig. 2).

To evaluate the on-site Coulomb repulsion U_{eff}, we use the linear response (LR) method [26]. In the LR approach, a perturbed repulsive Coulomb interaction is applied as a small shift of the potential on d levels such that the response of the system to this perturbation remains linear. Using the experimental structure of Sr_2NiWO_6, the U_{eff} converges to 6.2 eV for Ni, independent of magnetic ordering. Therefore, in the GGA+U calculations with the experimental structure we take the values 5, 6, and 7 eV for the Hubbard parameter.

To obtain consistent results in an *ab initio* theory, one needs to include all relevant details such as optimized structural geometry. Therefore, using the GGA+U, we optimize the structural geometry. For a fully consistent result, we also estimate U_{eff} in a self-consistent LR (SCLR) scheme [29]. For this purpose, in each step, the crystal structures are optimized in the GGA+U calculation with the value of the U parameter obtained from the previous step. Given the new structure, the value of U is updated in the SCLR scheme. Iterating this process makes the value of U converge to a constant. Starting from $U_{\text{eff}} = 6.2$ eV of the experimental structure, we find that the on-site Hubbard parameter converges to 4.72 eV. The total energy difference of the considered magnetic configurations and the FM state are reported in Fig. 2 for the experimental structure and *ab initio* optimized structure with $U_{\text{eff}} = 5$ eV and $U_{\text{eff}} = 4.72$ eV, respectively.

Now, we proceed to find the spin Hamiltonian. For this purpose, we map the resulting total energies onto the Heisenberg Hamiltonian. The relevant exchange constants (J_1, J_{1c}, J_2, J_{2c}) for the experimental structure with $U_{\text{eff}} = 0$, 5, 6, and 7 eV and the optimized structure with $U_{\text{eff}} = 4.72$ eV are listed in Table I, showing that all the couplings are AFM. The details of this calculation are given in the Appendix. The small difference between the energy of AFM-I and FM magnetic configurations (see Fig. 2) justifies the smallness of the inter-*ab* plane NN coupling J_{1c}. Indeed, one can simply find $J_{1c} = (E_{\text{AF-I}} - E_{\text{FM}})/8$.

Table I also shows that NNN coupling constants (J_2, J_{2c}) are an order of magnitude larger than the NN ones (J_1, J_{1c}). Indeed, the 90° Ni-W-Ni bond angle in both the intra- and inter-*ab* planes makes the superexchange interaction between the NN magnetic ions too weak. On the other hand, the Ni-W-Ni angle for both the intra- and inter-*ab* plane NNN ions is 180°, which substantially enhances the NNN exchange constants. Moreover, the Ni-O-W bond angle in the intra-*ab* plane (165.8°) is slightly smaller than the corresponding bond angle in the inter-*ab* plane (180°), which somewhat enhances J_{2c} compared with J_2. It can be seen from Table I that the coupling constants decrease by increasing U_{eff}, which is a consequence of attenuating the hopping amplitude of neighboring d electrons at the expense of enlarging the on-site Coulomb repulsion.

To check how the exchange constants depend on the method, we employ the LAPW method and compare its results to those obtained by PAW. For GGA (i.e., $U = 0$) there is a 10% (in average) discrepancy in the exchange constants between the two methods, which is reasonable. We repeat the LAPW calculation using GGA+U. It is worth mentioning that the GGA+U implementation in the FLEUR LAWP code

TABLE I. Obtained exchange constants (meV) and Néel temperature T_N (K) at different values of the Hubbard parameter (eV) for experimental and optimized crystal structures of Sr_2NiWO_6 within the PAW and LAPW methods. The calculations (PAW/GGA + U) with $U_{\text{eff}} = 0$, 5, 6, and 7 eV were done in the experimental structure and the one with $U_{\text{eff}} = 4.72$ eV corresponds to the optimized structure. All of the LAPW calculations have been done by using the experimental structure. The last row indicates the INS results for the exchange parameters [20]. For each exchange parameter set (except for the INS results), T_N is derived from MC simulations.

	U_{eff} (eV)	J_1 (meV)	J_{1c} (meV)	J_2 (meV)	J_{2c} (meV)	T_N (K)
PAW	0	−0.36	−0.34	−8.06	−9.07	139
	5	−0.16	−0.12	−3.06	−3.45	52
	6	−0.14	−0.10	−2.52	−2.83	43
	7	−0.11	−0.08	−2.05	−2.30	35
	4.72	−0.24	−0.05	−2.44	−2.90	43
LAPW	0	−0.54	−0.47	−8.22	−10.18	146
	5 ($U = 6.0, J_H$=1.0)	−0.27	−0.18	−1.87	−2.90	36
Expt. (INS) [20]		-0.02 ± 0.08		-1.81 ± 0.09		54 [18,19]

is based on Liechtenstein's approach [30], which includes two parameters: U as the on-site Coulomb repulsion and J_H as the on-site (Hund's) exchange. However, in the PAW/GGA+U method we employ Dudarev's approach [25], which uses only one parameter, i.e., U_{eff}. Generally, the relationship between U_{eff}, U, and J_H is $U_{\text{eff}} = U - J_H$. Knowing that in many oxides $J_H \sim 1$ eV [31,32], in this work we set J_H to 1 eV. In principle, one has to calculate U and J_H in LAPW/GGA+U, but as a rough approximation we use $U = U_{\text{eff}} + J_H$, where U_{eff} is the PAW value. The exchange parameters obtained by LAPW/GGA+U ($U = 6.0$, $J_H = 1.0$ eV) are reported in Table I. These results are comparable with those obtained by PAW when $U_{\text{eff}} = 5$–6 eV is used.

Linear spin-wave (LSW) fitting of the excitation spectrum obtained by the inelastic neutron scattering (INS) experiment results in $J_1 \approx -0.02$ meV and $J_2 \approx -1.81$ meV [20,21]. The discrepancy between our result and LSW comes from the linear approximation in LSW, which yields an error of the order of $1/S$ (which for $S = 1$ could be large). We will further discuss the INS result in Sec. III B.

Now we consider the biquadratic interaction between the NN along the inter-*ab* planes. The dependence of the total energy on the angle between the Ni magnetic moments reveals if there is a biquadratic interaction in this compound. The Ni^{+2} ions in Sr_2NiWO_6 are located in the lattice points of two tetragonal sublattices shifted by $(a/2, a/2, c/2)$. To calculate the biquadratic coupling constants B_{ij}, starting from a FM configuration, we compute the total energy of the magnetic configurations in which the directions of the magnetic moments in these two sublattices are rotated by the angle θ.

Figure 3 presents the variation of energy [$\Delta E = E(\theta) - E(\theta = 90^\circ)$] for GGA (i.e., $U_{\text{eff}} = 0$) and GGA+U ($U_{\text{eff}} =$ 5 eV) with the experimental structure. The ΔE-θ curve can be well fitted by the function $f(x) = 8(B\cos^2\theta - J_{1c}\cos\theta)$, which comes from the spin Hamiltonian containing only the inter-*ab* plane NN Heisenberg and biquadratic interactions (the NNN interactions do not have any contribution in ΔE). As a result, there is a biquadratic interaction in Sr_2NiWO_6 in both GGA and GGA+U. The biquadratic coupling constant is negative and its value is $B \approx -0.03$ and -0.04 meV for $U_{\text{eff}} = 0$ and 5 eV, respectively. Similar results are obtained if we use the optimized crystal structure with $U_{\text{eff}} = 4.72$ eV.

Finally, we investigate the single-ion anisotropy arising from the spin-orbit effect. The single-ion term can be written as $\Delta \sum_i (\hat{\mathbf{n}}_i \cdot \hat{\mathbf{d}})^2$, where $\hat{\mathbf{d}}$ denotes the easy-axis direction. We assume that $\hat{\mathbf{d}}$ is along the lattice c axis (see Fig. 1). Using GGA+U+SOC with $U_{\text{eff}} = 5$, we calculated the total energy for the FM spin configuration as the angle θ (the angle between the magnetic moment direction and the z axis) varies from 0 to π. Figure 4 shows the variation of ΔE vs θ. This figure represents that the minimum energy is achieved at $\theta = 0$. The value of Δ from this calculation is ≈ -0.05 meV, whose sign indicates that the z axis is indeed an easy axis. We also checked that the total energy is independent of the azimuthal angle ϕ. It should be noted that the two-spin Ising anisotropy ($J_z S_{i,z} S_{j,z}$) may make a contribution to the energy difference curve in Fig. 4. Nevertheless, it is hard to separate its contribution since both single-ion and Ising anisotropy terms have the same angular dependence for a uniform rotation of the spin direction. Due to this limitation we assign it totally to the single-ion anisotropy.

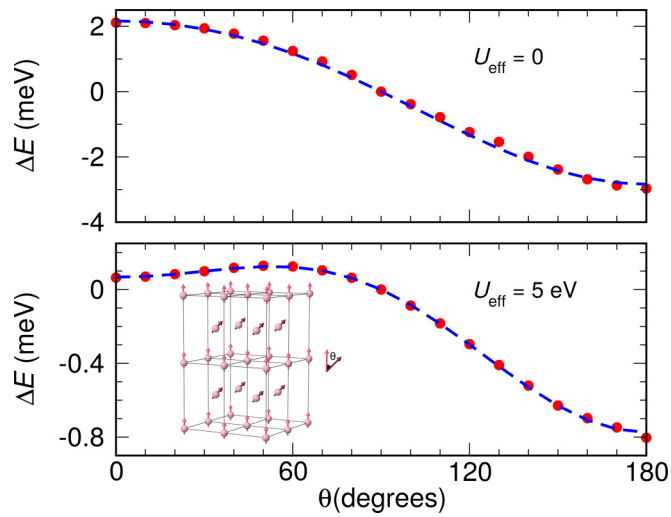

FIG. 3. Total energy vs rotational angle θ (the angle between the magnetic moments of the two tetragonal sublattices). The reference of energy is set to $\theta = 90^\circ$. The dashed line denotes the fit to the data using the function $f(x) = 8(B\cos^2\theta - J_{1c}\cos\theta)$.

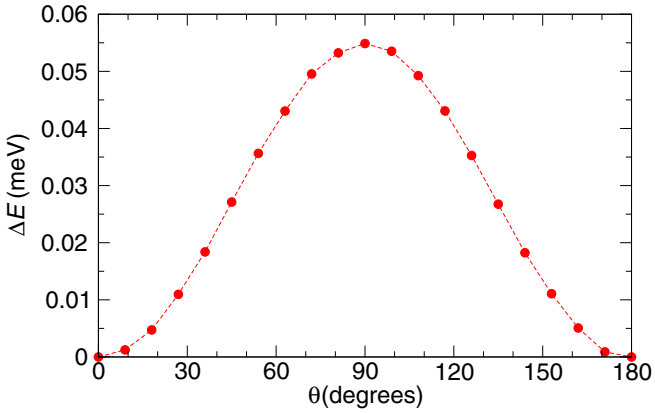

FIG. 4. Total energy vs rotational angle θ with respect to the lattice c axis within GGA+U+SOC. The reference of energy is set to $\theta = 0^\circ$.

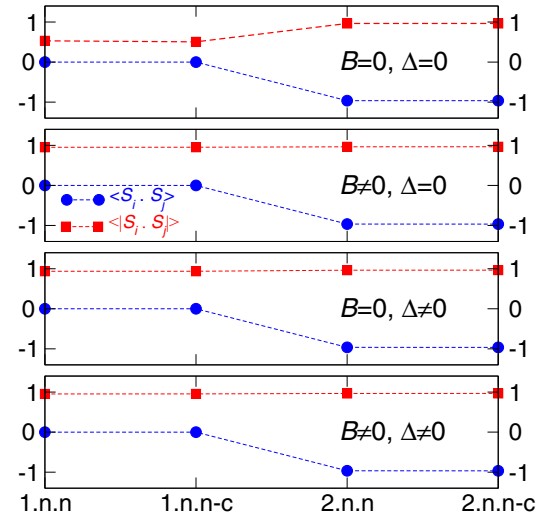

FIG. 5. Average (absolute) spin-spin correlation of intra- and inter- *ab* plane NN and NNN obtained by MC simulations at $T = 4$ K with the derived exchange parameters using $U_{\text{eff}} = 5$ eV.

B. Monte Carlo simulation

To investigate the finite-temperature behavior of the spin Hamiltonian, we carry out classical MC simulations, using the coupling constants obtained by $U_{\text{eff}} = 0$, 5, 6, and 7 eV in the experimental and $U_{\text{eff}} = 4.72$ eV in the optimized structure. It is found that all the spin Hamiltonians, containing NN and NNN Heisenberg couplings (given in Table I) and NN inter-*ab* plane biquadratic terms ($B = J_{1c}$), in both experimental and optimized structures, and the exchange couplings show a transition to an AFM-II ordering with the Néel temperatures (T_N) given in Table I. Comparing the measured $T_N \approx 54$ K [18,19], we find that taking $U_{\text{eff}} \approx 5$ eV would be fine choice for the experimental structure. Moreover, in the optimized structure, the T_N obtained by the SCLR value $U_{\text{eff}} = 4.72$ eV is in good agreement with the experimentally measured value. The SCLR method gives reasonable results for the compounds whose bonds have a high ionic character. Using the CRITIC2 code [33,34], we find the following valence state based on a Bader charge analysis: $Sr_2{}^{+1.60}Ni^{+1.39}W^{+3.00}O_6{}^{-1.26}$. The charge analysis shows that the nature of the Ni-O bonds in Sr_2NiWO_6 is predominantly ionic, which is the reason that SCLR works for this compound.

The exchange constants obtained by INS result in $T_N = 34$ K in a MC simulation which is 40% less than experimental value T_N (54 K). This discrepancy, as already discussed, could be due to using the LSW for $S = 1$ which underestimates the value of J_2.

It should be mentioned that the biquadratic and single-ion interactions do not have much of an effect on T_N, nevertheless, we will show in the following that they have an essential role in singling out a collinear spin configuration.

To gain insight into the low-temperature magnetic ordering in the MC simulations, we calculate the average spin-spin correlation at $T = 4$ K. Figure 5 represents the averages of the products of the neighboring spins ($\langle S_i \cdot S_j \rangle$) and also their absolute values ($\langle |S_i \cdot S_j| \rangle$) for the spin Hamiltonian given by the couplings obtained by $U_{\text{eff}} = 5$ eV. As can be seen from this figure, regardless of the absence or presence of the biquadratic and single-ion interactions, $\langle S_i \cdot S_j \rangle$ is ≈ 0 for both intra- and inter-*ab* plane NN spins and ≈ 1 for all NNN spins. However, for the NN spins the value of $\langle |S_i \cdot S_j| \rangle$ is less than 1 (≈ 0.5) in the absence of a biquadratic term or single-ion term and about 1 when including one or both of these interactions ($B \approx -0.04$, $\Delta \approx -0.05$ eV). These calculations show that when both B and Δ are zero, the magnetic moments have the freedom to rotate with respect to their nearest neighbors, however, when either B or Δ is turned on, they lose their freedom and fix their directions parallel or antiparallel to their neighbors, hence stabilizing the collinear configuration AFM-II. Indeed, the freedom of the magnetic moments to rotate would give rise to a residual entropy at low temperatures, however, the experimental results do not show such an entropy [19].

Our MC simulations show that the ground state of Sr_2NiWO_6 is doubly degenerate. This can be verified by calculating the elastic neutron scattering structure function given by

$$S(\mathbf{q}) = \sum_{i;j} \left\langle \left(\mathbf{S}_i - \frac{\mathbf{S}_i \cdot \mathbf{q}}{\mathbf{q} \cdot \mathbf{q}} \mathbf{q} \right) \cdot \left(\mathbf{S}_j - \frac{\mathbf{S}_j \cdot \mathbf{q}}{\mathbf{q} \cdot \mathbf{q}} \mathbf{q} \right) \right\rangle \times \exp[i\mathbf{q} \cdot (\mathbf{R}_i - \mathbf{R}_j)]. \quad (2)$$

Indeed, different MC runs end in two collinear spin configurations AFM-II and AFM-IIb illustrated in Fig. 6. The difference between these two configurations is the rotation of the (0,0,2) planes (highlighted in gray) by 90° with respect to the (0,0,1) planes along the c direction. The right panels in Fig. 6 show the density plots of $S(\mathbf{q})$ for these two spin configurations. The main difference between the pattern of $S(\mathbf{q})$ for these two spin configurations is the elimination of some Bragg peaks in AFM-II.

While AFM-II and AFM-IIb are classically degenerate, it has been shown that in a large S limit the quantum effects lift the degeneracy of these two magnetic configurations in favor of AFM-II [35].

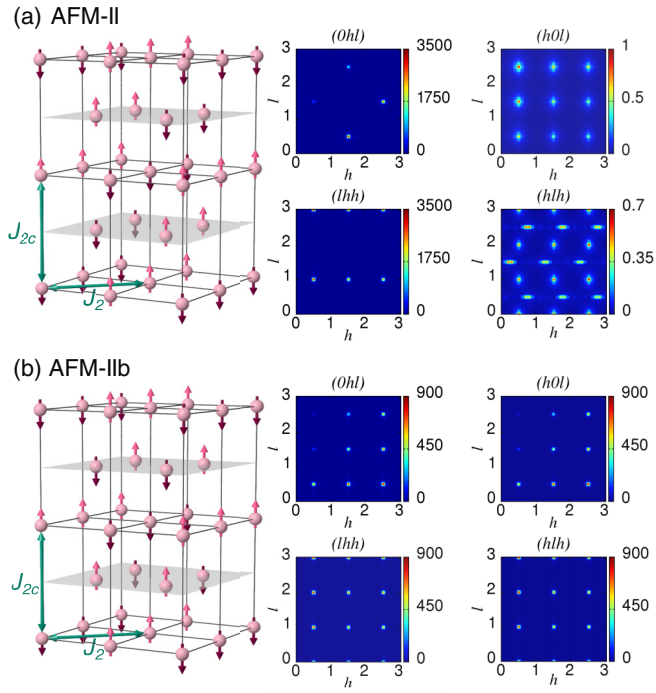

FIG. 6. A schematic of the type-II antiferromagnetic (AFM-II) and type-IIb antiferromagnetic (AFM-IIb) ordering and their MC neutron structure factor $S(\mathbf{q})$ in the $(0hl)$, $(h0l)$, (lhh), and (hlh) planes at $T = 4$ K by including the Heisenberg, biquadratic, and anisotropy terms in the spin Hamiltonian which is derived from GGA+U ($U_{\text{eff}} = 5$ eV).

IV. CONCLUSIONS

In summary, we studied the magnetic interactions and thermodynamic properties of Sr_2NiWO_6, using *ab initio* GGA and GGA+U calculations and classical Monte Carlo simulations. We found that interactions of the next-nearest neighbors in the intra- and inter-*ab* plane, the biquadratic interaction between the inter-*ab* plane nearest neighbors, and the magnetic anisotropy along the $\hat{\mathbf{z}}$ are the key players in determining the magnetic ordering of this compound. Our results show that the classical ground state of Sr_2NiWO_6 has a double degeneracy denoted by AFM-II and AFM-IIb. The elastic neutron scattering structure factors corresponding to these two magnetic configurations were calculated and presented as reliable theoretical references for the experimental refinement of the true magnetic ground state of this compound by using neutron scattering experiments.

ACKNOWLEDGMENTS

N.R. and H.A. acknowledge the support of the National Elites Foundation and Iran National Science Foundation (INSF). We acknowledge Hojjat Gholizadeh for his help in using POV-Ray.

TABLE II. The total energy difference of different magnetic configurations (meV/f.u.) with respect to the ferromagnetic configuration within GGA+U/PAW and the Heisenberg model. For GGA+U/PAW, we used an optimized structure with $U_{\text{eff}} = 4.72$ eV. For the Heisenberg model, we used exchange parameters from an optimized structure of GGA+U/PAW with $U_{\text{eff}} = 4.72$ eV.

Method	GGA+U/PAW	Heisenberg model
AFM-I	− 0.544	− 0.368
AFM-II	− 16.264	− 16.217
AFM-III	− 7.068	− 6.954
AFM-IV	− 1.071	− 1.147
AFM-V	− 5.848	− 5.991
AFM-VI	− 10.440	− 10.410
AFM-VII	− 5.759	− 5.778
AFM-VIII	− 5.544	− 5.584
AFM-IX	− 7.956	− 7.974
AFM-X	− 2.817	− 2.953
AFM-XI	− 3.051	− 3.087

APPENDIX: DETAILS ABOUT THE TOTAL ENERGIES OF ALL OUR CONFIGURATIONS

The total energies for eight formula units without considering the nonmagnetic part, by the Heisenberg Hamiltonian for ferromagnetic ordering, can be written as

$$E_{\text{FM}} = (32J_1 + 64J_{1c} + 32J_2 + 16J_{2c})S^2, \qquad \text{(A1)}$$

and for the considered AFM orderings as

$$\begin{aligned}
E_{\text{I}} &= (32J_1 - 64J_{1c} + 32J_2 + 16J_{2c})S^2,\\
E_{\text{II}} &= (0J_1 + 0J_{1c} - 32J_2 - 16J_{2c})S^2,\\
E_{\text{III}} &= (-32J_1 + 0J_{1c} + 32J_2 - 16J_{2c})S^2,\\
E_{\text{IV}} &= (-32J_1 + 0J_{1c} + 32J_2 + 16J_{2c})S^2,\\
E_{\text{V}} &= (32J_1 + 0J_{1c} + 32J_2 - 16J_{2c})S^2,\\
E_{\text{VI}} &= (0J_1 + 0J_{1c} - 32J_2 + 16J_{2c})S^2,\\
E_{\text{VII}} &= (-16J_1 + 0J_{1c} + 0J_2 + 16J_{2c})S^2,\\
E_{\text{VIII}} &= (0J_1 - 16J_{1c} + 0J_2 + 16J_{2c})S^2,\\
E_{\text{IX}} &= (0J_1 + 0J_{1c} - 16J_2 + 16J_{2c})S^2,\\
E_{\text{X}} &= (16J_1 - 32J_{1c} + 16J_2 + 16J_{2c})S^2,\\
E_{\text{XI}} &= (32J_1 + 0J_{1c} + 32J_2 + 0J_{2c})S^2.
\end{aligned}$$

In Table II we gather and compare the GGA+U/PAW total energies with their counterpart Heisenberg Hamiltonians. The mean absolute error of the Heisenberg Hamiltonian energy with respect to the GGA+U/PAW total energy is about 0.07 meV/f.u.

[1] S. Vasala and M. Karppinen, Prog. Solid State Chem. **43**, 1 (2015).

[2] C. J. Howard, B. J. Kennedy, and P. M. Woodward, Acta Crystallogr., Sect. B **59**, 463 (2005).

[3] A. Hossain, P. Bandyopadhyay, and S. Roy, J. Alloys Compd. **740**, 414 (2018).
[4] S. Vasala, H. Saadaoui, E. Morenzoni, O. Chmaissem, T.-S. Chan, J.-M. Chen, Y.-Y. Hsu, H. Yamauchi, and M. Karppinen, Phys. Rev. B **89**, 134419 (2014).
[5] T. Kimura, H. Sawada, and K. Terakura, Nature (London) **395**, 677 (1998).
[6] J. B. Philipp, P. Majewski, L. Alff, A. Erb, R. Gross, T. Graf, M. S. Brandt, J. Simon, T. Walther, W. Mader *et al.*, Phys. Rev. B **68**, 144431 (2003).
[7] H. Hsu, P. Blaha, and R. M. Wentzcovitch, Phys. Rev. B **85**, 140404 (2012).
[8] S. Kumar, G. Giovannetti, J. van den Brink, and S. Picozzi, Phys. Rev. B **82**, 134429 (2010).
[9] A. Prasatkhetragarn, S. Kaowphong, and R. Yimnirun, Appl. Phys. A **107**, 117 (2012).
[10] A. A. Gusev, S. I. Raevskaya, V. V. Titov, V. P. Isupov, E. G. Avvakumov, I. P. Raevski, H. Chen, C.-C. Chou, S. P. Kubrin, S. V. Titov *et al.*, Ferroelectrics **496**, 231 (2016).
[11] V. V. Laguta, V. A. Stephanovich, M. Savinov, M. Marysko, R. O. Kuzian, I. V. Kondakova, N. M. Olekhnovich, A. V. Pushkarev, Y. V. Radyush, I. P. Raevski *et al.*, New J. Phys. **16**, 113041 (2014).
[12] R. Nechache, W. Huang, S. Li, and F. Rosei, Nanoscale **8**, 3237 (2016).
[13] T.-Y. Cai, S.-C. Liu, S. Ju, C.-Y. Liu, and G.-Y. Guo, Phys. Rev. Appl. **8**, 034034 (2017).
[14] D. Iwanaga, Y. Inaguma, and M. Itoh, J. Solid State Chem. **147**, 291 (1999).
[15] J. B. Goodenough, Phys. Rev. **100**, 564 (1955).
[16] J. Kanamori, J. Phys. Chem. Solids **10**, 87 (1959).
[17] G. Blasse, J. Phys. Chem. Solids **26**, 1969 (1965).
[18] D. Iwanaga, Y. Inaguma, and M. Itoh, Mater. Res. Bull. **35**, 449 (2000).
[19] C. G. F. Blum, A. Holcombe, M. Gellesch, M. I. Sturza, S. Rodan, R. Morrow, A. Maljuk, P. Woodward, P. Morris, A. U. B. Wolter *et al.*, J. Cryst. Growth **421**, 39 (2015).
[20] Y. Todate, J. Phys. Chem. Solids **60**, 1173 (1999).
[21] Y. Todate, Activity Report on Neutron Scattering Research **2**, 127 (1995), ISSP (unpublished).
[22] D. K. Buck and A. A. Collins, http://www.povray.org/.
[23] P. Giannozzi, S. Baroni, N. Bonini, M. Calandra, R. Car, C. Cavazzoni, D. Ceresoli, G. L. Chiarotti, M. Cococcioni, I. Dabo *et al.*, J. Phys.: Condens. Matter **21**, 395502 (2009).
[24] J. P. Perdew, K. Burke, and M. Ernzerhof, Phys. Rev. Lett. **77**, 3865 (1996).
[25] S. L. Dudarev, G. A. Botton, S. Y. Savrasov, C. J. Humphreys, and A. P. Sutton, Phys. Rev. B **57**, 1505 (1998).
[26] M. Cococcioni and S. de Gironcoli, Phys. Rev. B **71**, 035105 (2005).
[27] FLEURgroup, http://www.flapw.de/.
[28] F. Patrik, *Lecture Notes on Electron Correlation and Magnetism* (World Scientific, Singapore, 1999), Vol. 5.
[29] H. J. Kulik, M. Cococcioni, D. A. Scherlis, and N. Marzari, Phys. Rev. Lett. **97**, 103001 (2006).
[30] A. I. Liechtenstein, V. I. Anisimov, and J. Zaanen, Phys. Rev. B **52**, R5467 (1995).
[31] V. I. Anisimov, J. Zaanen, and O. K. Andersen, Phys. Rev. B **44**, 943 (1991).
[32] L. Vaugier, H. Jiang, and S. Biermann, Phys. Rev. B **86**, 165105 (2012).
[33] A. O. de-la Roza, E. R. Johnson, and V. Luaña, Comput. Phys. Commun. **185**, 1007 (2014).
[34] A. O. de-la Roza, M. Blanco, A. M. Pendás, and V. Luaña, Comput. Phys. Commun. **180**, 157 (2009).
[35] T. Yildirim, A. B. Harris, and E. F. Shender, Phys. Rev. B **58**, 3144 (1998).